Proceedings of
11th European Conference on Turbomachinery Fluid dynamics & Thermodynamics
ETC11, March 23-27, 2015, Madrid, Spain

Analysis of the influence of periodic passing wakes on the secondary flow near the endwall of a linear LPT cascade using DNS and U-RANS

D. Koschichow, J. Fröhlich

Institute of Fluid Mechanics
TU Dresden
Georg-Bähr-Str. 3c
01062 Dresden, Germany
Email: denis.koschichow@tu-dresden.de

R. Ciorciari, R. Niehuis

Institute of Jet Propulsion
Universität der Bundeswehr München
Werner-Heiseberg-Weg 39
85577 Neubiberg, Germany
Email: roberto.ciorciari@unibw.de

ABSTRACT

The paper presents an analysis of the impact of periodically passing wakes on the secondary flow near the endwall in a linear aft-loaded T106 low-pressure turbine cascade. Highly resolved Direct Numerical Simulations (DNS) and unsteady Reynolds Averaged Navier-Stokes (U-RANS) simulations were carried out to capture the transient turbulent motion and periodic components of the flow in detail. The Reynolds number is 90,000 based on the chord length and the exit flow velocity. The evolution of the boundary layers along the endwall are addressed with time-averaged and phase-averaged results. The present paper is one of the first to address this topic by means of DNS.

In front of the cascade, both DNS and U-RANS yield very similar results concerning the impact of the incoming wakes on the endwall boundary layer. In the passage, the endwall flow computed with both approaches is different, though. It remains unaffected by the wakes in the DNS while an impact is predicted with U-RANS. Furthermore, the endwall boundary layer exhibits differences in shape factor and turbulent kinetic energy.

NOMENCLATURE

Latin Symbols

c	chord
H	blade span
H_{12}	shape factor
h	half blade span, $H/2$
L	length
Ma	Mach number
Re	Reynolds number
Sr	Strouhal number, $(v_{bar}/t_{bar}) \cdot (c/v_{ax0})$
T	Bar passing period, t_{bar}/v_{bar}
t	pitch, time
v	velocity
x	axial coordinate
$y, u/t$	pitch-wise coordinate
$z, z/h$	span-wise coordinate

Greek Symbols

α	angle of the velocity vector to the x-axis
δ	boundary layer thickness
δ_1	displacement thickness
δ_2	momentum thickness
$\Delta\beta_{2,sec}$	exit flow angle deviation
ζ_2	Total pressure losses
μ, ν	dynamic viscosity, kinematic viscosity
τ_w	wall shear stress
ϕ	flow coefficient, v_{ax}/v_{bar}
Φ	phase of time period T
ω	vorticity

Abbreviations

CFD	Computational Fluid Dynamics
DNS	Direct Numerical Simulation
EXP	Experimental
LES	Large Eddy Simulation
LPT	Low Pressure Turbine
RANS	Reynolds Averaged Navier-Stokes
TKE	Turbulent Kinetic Energy

subscripts

0	inlet plane upstream the cascade
ax	axial
n	direction normal to a streamline
ref	reference value
steady	steady calculations results
t	direction tangential to a streamline
th	theoretical
z	span-wise

INTRODUCTION

In the last years, turbine design has become a mature field and relevant gains in performance and efficiency are becoming more difficult with traditional design methods. Nowadays, focus for design improvements are put on secondary flows and unsteady interaction effects in turbomachinery that lead to new requirements for the experimental and computational design methods (Tyacke *et al.*, 2013). The typical experimental methods are limited by the access restrictions in test rigs, by the safety environmental issues and by the economic costs. On the other hand, the commonly used three-dimensional Reynolds-Averaged Navier-Stokes (RANS) models, which are having a relevant impact on all aspects of turbomachinery design, are not able to accurately predict a wide range of aerodynamic turbulent flows with a large-scale separation or with a relevant unsteadiness (Travin *et al.*, 2004). Consequently, an innovative and more reliable approach is needed to improve the design methods and to control unsteady flow effects. The use of U-RANS methods could bridge the gap to the time-resolved mode in a Navier-Stokes solver and to resolve low frequency unsteadiness, as DNS, LES and hybrid methods are still not considered to be applicable in the routine design practice (Travin *et al.*, 2004; Tucker, 2011). The U-RANS approach is recognized as a useful method to describe and to better understand the unsteady flows in turbomachinery. Despite the uncertainties, which U-RANS simulation have, this method is widely used in connection with experimental measurements to study unsteady secondary flow effects (Denton and Pullan, 2012; Holley *et al.*, 2006; Lei *et al.*, 2010). However, the relative limits must be taken into account and evaluated. Comparisons of U-RANS with DNS or LES predictions are useful to assess the limits of the Reynolds averaged formulation and the therefore required turbulence models. Recently, the weakness of the turbulence models based on the Boussinesq viscosity assumption in RANS formulation was investigated and quantified by Michelassi *et al.* (2014) in a DNS study. Moreover, a comparative study of aerodynamics and heat transfer on a highly loaded turbine blade using U-RANS, LES, and experimental results was performed by Schobeiri and Nikparto (2014). Stating that the deficiencies of existing RANS-based numerical methods are due to an inadequate modeling of the dissipation equation and the lack of a better transition model. In turbine cascades, the boundary layer near the endwall is characterized by separation as well as by the interaction of the viscous wall flow with vortices which are driven and generated by the pressure gradient. An appropriate analysis of the main properties of the endwall flow and the related endwall loss generation mechanisms in a turbine cascade is strictly conditioned by the modeling of the transitional and turbulent flow (Denton and Pullan, 2012). Considering an unsteady flow behaviour, the transitional flow behavior and the unsteadiness introduced by incoming wakes or streamwise vorticity increase the complexity of this kind of flows. In this context a comparison of the endwall flow obtained by U-RANS and DNS predictions is useful to assess both methods in terms of their capabilities for practiced unsteady turbomachinery flows.

In previous works by Koschichow *et al.* (2014) and Ciorciari *et al.* (2014), it was found that periodic wakes have only small influence on the flow at the outlet of the cascade. This applies for experimental measurement as well as for numerical investigations by DNS and U-RANS simulations. The reason was suspected to reside in the fact that the incoming boundary layer in the studied configuraton is quite thin, and the background turbulence relatively strong. Both are detected by the experimental setup. In these investigations, the influence of the periodic wakes on the formation of the horseshoe vortex and the passage vortex downstream of the cascade was studied. The question about the effect

of the periodic disturbances introduced by the incoming wakes on the development of the endwall boundary layer remained largely unanswered. The goal of the present work is to address this issue and to reach a better understanding of the influence of periodic passing wakes on the endwall flow in the investigated linear LPT. Experimental data for the velocity are not available inside the passage, so that the DNS data are used to study the impact of the upstream wakes on the complex flow physics near the endwall. Furthermore, the DNS results are also compared to U-RANS predictions. By doing so, the limitations of the U-RANS method can be evaluated and its suitability for the simulation of this kind of flow assessed.

Investigated configurations

The DNS and the U-RANS simulations with and without incoming wakes were carried out for the flow through a linear aft-load T106 LPT cascade. They are based on the experimental investigations performed in the High Speed Cascade Wind Tunnel of the Institute of Jet Propulsion of the University of the German Federal Armed Forces Munich (Universität der Bundeswehr München). More information and details of the reference test rig are described in (Ciorciari *et al.*, 2014). Figure 1 shows a sketch of the configuration of the tested cascade. Table 1 summarizes the cases investigated with periodic incoming wakes. For these investigations, the theoretical cascade exit Mach number and the Reynolds number are $Ma_{2th} = 0.40$ and $Re_{2th} = 9 \cdot 10^4$, respectively. In addition to the parameters introduced in the Figure 1, the inlet velocity and the velocity of the periodic passing wakes are $v_{in} = 75\,m/s$ and $v_{bar} = 20\,m/s$, so that the flow coefficient is $\phi \approx 3$ in all cases. In addition to these cases with impinging wakes, the same configuration without wakes but the same background turbulence according to the experimental conditions was investigated and will be labeled *Tnw* (*nw*=no wakes) with all other parameters unchanged. All investigated configurations are characterized by an incoming boundary layer smaller than 6% of the half span of the profile.

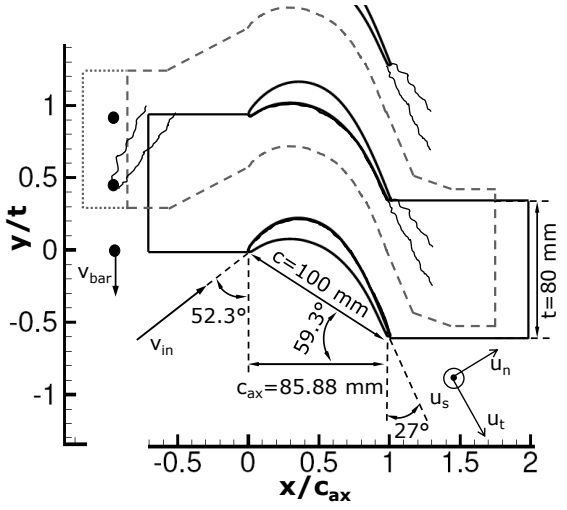

Figure 1: **Sketch of the configuration and computational domain for DNS (solid line), RANS (dashed line) and U-RANS (dashed + dotted lines).** $L_z = 0.99 c_{ax}$ **in both cases.**

Conf.	$t_{bar}[mm]$	Sr	Ma_{2th}
Tnw RANS	-	-	0.4
T80-20 URANS	80	0.40	0.4
T40-20 URANS	40	0.79	0.4
Tnw DNS	-	-	0
T40-20 DNS	40	0.79	0
Tnw EXP	-	-	0.4
T80-20 EXP	80	0.40	0.4

Table 1: **Cases investigated.**

Conf.	$n_{tot} \cdot 10^6$	$\triangle\, t \cdot 10^{-7}\ s$
DNS	≈ 212	≈ 1
RANS	≈ 3.5	≈ 50

Table 2: **Total number of grid points and size of time step in the simulation conditioned.**

NUMERICAL SETUP

Flow solvers

Both simulation approaches are described and extensively validated for the present configuration by comparison to experimental data in previous publications: Koschichow *et al.* (2014) for DNS and

Ciorciari *et al.* (2014) for U-RANS to which we refer here. The DNS were computed with the research code LESOCC2 (Hinterberger *et al.*, 2008) applying a cell-centered second-order finite volume multi-block method for the spatial discretization and a second-order predictor-corrector method in time. The TRACE code (Yang *et al.*, 2002, 2006) employed for the U-RANS simulations uses a second-order finite volume approach on a multiblock-structured grid with an implicit dual-time stepping technique. The fluid is compressible in the U-RANS simulations, while treated as incompressible in the DNS.. For the U-RANS a $k-\omega$ turbulence model with a $\gamma - Re_{\theta t}$ transition model is used (Marciniak *et al.*, 2010).

Boundary conditions, computational domains and parameters

To compare the results obtained by U-RANS and DNS, the differences of the boundary conditions and domain modelling must be taken into account. The computational domains of both simulations are shown in Figure 1 with mesh resolution and time step listed in Table 2. The size of the domain in the spanwise direction is $L_z = 0.99\, c_{ax}$ for both, DNS and U-RANS. For the DNS, the position of the inflow plane was selected according to the location where the velocity measurements were taken in the experiment, i.e. the plane at $x = -0.6\, c = -0.699\, c_{ax}$. Mean velocities were imposed according to the experimentally measured mean values. The generation of the inlet conditions in the case with periodical incoming wakes was obtained for the DNS by superimposing independently generated turbulent boundary layer data and data from the bar wakes. For the latter, data were adopted from Wissink and Rodi (2008), who performed a DNS of the flow around a circular cylinder, and were rescaled to match the experimental level. Boundary layer data were generated so as to match the measured amount of fluctuations employing the procedure of de Meux *et al.* (2012).
For the RANS and U-RANS the inlet of the cascade is at $x = -0.7\, c = -0.815\, c_{ax}$ in front of the leading edge of the blades. The inlet total pressure and temperature in the RANS simulation were imposed at this plane. The periodical wake inflows in the U-RANS calculations were produced with two additional blocks in front of the cascade to generate the required unsteady inflow conditions as described in (Ciorciari *et al.*, 2014).
The outlet plane in the DNS, located at a distance of $1\, c_{ax}$ from the airfoil trailing edge, is characterized by a convective outflow condition. In the RANS/U-RANS, static pressure nonreflecting outflow boundary condition were used at $0.75\, c_{ax}$ downstream of the trailing edge. For both simulation types, a no-slip condition was imposed on the walls and a symmetry plane was applied at midspan to reduce the computational effort. In order to reduce the computation time, the Strouhal number simulated by the DNS is higher by a factor of two compared to the experiment.

RESULTS

Overview

The analysis of the predicted results and endwall boundary layers will be presented in three steps. First, the two prediction approaches will be compared to experimental data, with parts of the results already shown in (Koschichow *et al.*, 2014). Subsequently a discussion of the time-averaged results of the U-RANS simulations and the DNS will be provided for steady and unsteady configurations. Finally, phase-averaged data for the *T40-20* configuration will be presented. A determination of the boundary layer parameters is not trivial for a complex three-dimensional flow with secondary flow like the one in the leading edge region shown in Figure 2. The black streamlines near the endwall show a highly complex near-wall flow with a stagnation point and local flow reversal, while the bright streamlines illustrate the outer flow. Consequently, the free stream flow velocity is not suitable to define the endwall boundary layer thickness and the relative parameters in this region. Hence, an alternative vorticity-based definition proposed by Michelassi *et al.* (1999) is applied to define the boundary layer thickness in the turbine cascade endwall region. First, the local velocity vectors in

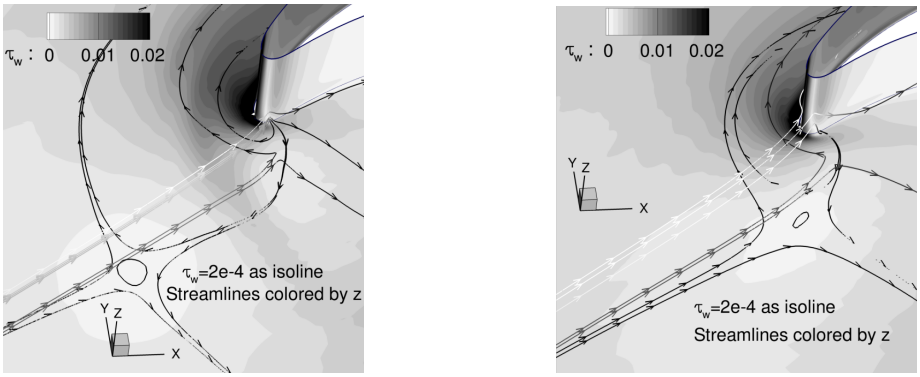

(a) (b)

Figure 2: **Three-dimensional time-averaged flow visualized by means of streamlines colored by the z-coordinate: (a) DNS without wakes, (b) DNS with wakes, case *T40-20*. The contour plot on the endwall and blade surface reports the dimensionless wall-shear stress.**

each *x*-*y*-plane are decomposed into a tangential and a normal component, u_t and u_n, respectively. The wall shear stress is always oriented in tangential direction, so that $\tau_w = \rho\nu\partial u_t/\partial z$ is always positive. Then, the vorticity vector is decomposed in the same way, and the boundary layer thickness δ detected by solving the equation:

$$\omega(\delta) = \omega_{n,min} + 0.01(\omega_{n,max} - \omega_{n,min})$$

for δ. Finally, the shape factor $H_{12} = \delta_1/\delta_2$ is calculated in the entire passage to characterize the endwall boundary layer with the the displacement thickness and the momentum thickness of the boundary layer computed as

$$\delta_1 = \int_0^\delta \left(1 - \frac{u_t(z)}{u_\delta}\right) dz \quad \text{and} \quad \delta_2 = \int_0^\delta \frac{u_t(z)}{u_\delta}\left(1 - \frac{u_t(z)}{u_\delta}\right) dz$$

using the vorticity-based boundary layer thickness δ.

Comparison with experimental data downstream the cascade

The measured spanwise distributions of the pitchwise averaged exit flow angle deviation $\Delta\beta_{2,sec}$ and the total pressure loss coefficient ζ_2 downstream the cascade at $x/c_{ax} = 1.47$ are used to evaluate the reliability and to make first comparisons between the predicted results. In Figure 3 the investigated cases with and without incoming wakes are compared.

In the compressible RANS/U-RANS predictions the location of the underturning peaks around $z/h = 0.3$ are well captured. The same is valid for the total pressure losses, the spanwise position of the local maximum in the underturning region and the local minimum between $z/h = 0.1$ and $z/h = 0.15$ are similar to the measured data. Some differences are to be found in the local loss intensity for the *Tnw* RANS at $z/h = 0.5$, where the trailing edge wake vortex interacts with the cascade profile wake, and at $z/h = 0.15$, where the passage vortex interact, with the corner vortex. In the *T80-20* U-RANS calculations, the mentioned interaction regions show a better agreement with the experiments, but in the underturning region the local loss peak is more intense.

In Figure 3, the DNS data show a good qualitative reproduction of the measured data taking into account the impact of the compressibility. The spanwise shifting in the midspan direction of the loss cores and the more intense under- and overturning in the DNS result from the compressibility effect

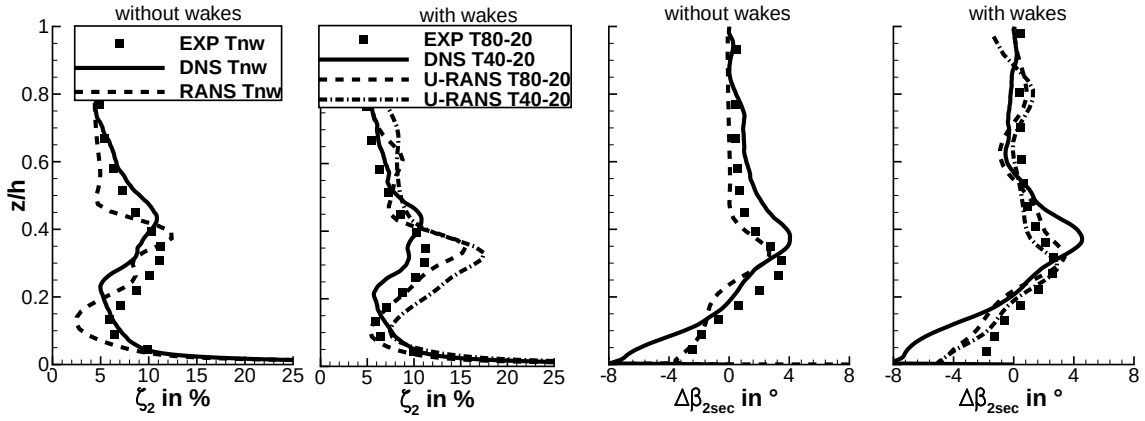

Figure 3: **Comparison of EXP, DNS and U-RANS by means of time-averaged and pitch-averaged values at the outlet,** $x/c_{ax} = 1.47$ **for the case *Tnw* and the cases *T80-20* and *T40-20*. The left two pictures show the total loss coefficient** ζ_2**. The right two pictures show the exit flow angle deviation** $\Delta\beta_{2,sec}$**.**

on the secondary flow the cascade (Perdichizzi, 1986). The pitchwise averaged intensity of the losses, the interactions in the secondary and wake region downstream the cascade are predicted correctly. While the DNS of the incompressible flow and the U-RANS with its models could not exactly match the experiment the qualitative impact of the wakes on the flow can be predicted well.

Time-averaged quantities

To analyze the main differences near the endwall between the DNS and U-RANS approach for the steady and unsteady configurations, a first comparison of time-averaged predicted data are plotted in Figure 4 and 5. For the both undisturbed *Tnw* configurations (Figure 4a and 5a), the small incoming laminar boundary layer grows in thickness and remain laminar until the entrance into the cascade passage. There, the incoming boundary layers are affected by the nonuniform pitchwise pressure fields caused by the presence of the blades. In front of the leading edge of the blade near the endwall, the saddle point can be identified by two incoming and two outgoing streamlines in Figure 4. Between the saddle point and the leading edge, an area of increased shape factor can be observed caused by the roll-up of the horseshoe vortex. The horseshoe vortex is weak for the investigated configurations, as quantified through the Ekerle-Awad parameter in (Koschichow *et al.*, 2014), but the value $H_{12} = 4$, seen in the DNS, indicates that the flow tends to separate (Kožulović, 2007). The so-called horseshoe/passage vortex "lift-off line" (Harrison, 1989) is identified by means of the two streamlines going out from the saddle point, see Figure 4. In the following the outgoing streamline towards the suction side of the adjacent blade is "lift-off line".

In all predictions downstream of the "lift-off line", a turbulent region with $H_{12} \approx 1.5$ can be observed between the pressure side and the suction side in Figure 4 and 5. Particularly in the DNS of case *Tnw* in Figure 4a, this is reflected by a small band across the passage at $x \approx 0.25\, c_{ax}$. For the steady *Tnw* RANS in Figure 5a, the turbulent area starts at the same axial position but its downstream extension is larger than in the DNS.

After the turbulent strip near the endwall the pressure gradient between the pressure and the suction side induces a strong crossflow. The boundary layer generated by this "endwall crossflow" (Langston, 1980) is computed differently by DNS and RANS/U-RANS. In the DNS, a rapid increase of the shape factor to the value $H_{12} \geq 2.3$ indicates a crossflow endwall boundary layer with a laminar characteristic. In the RANS result, the shape factor H_{12} remains around 1.4 in large area extending further

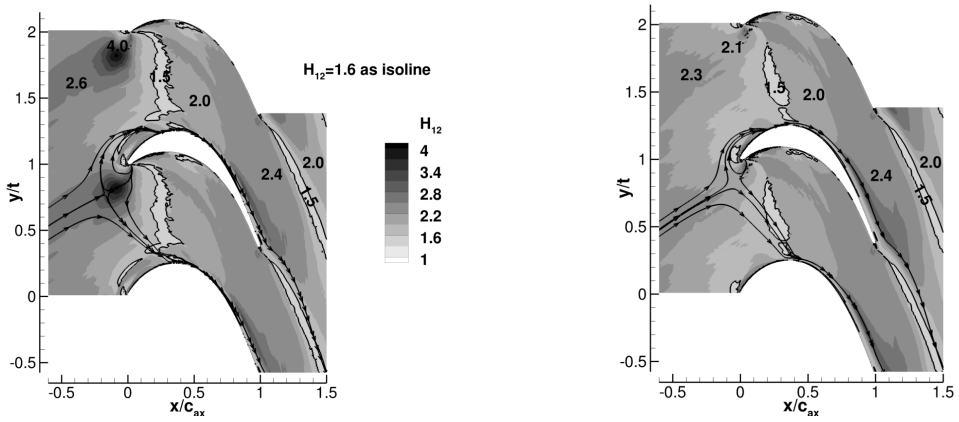

Figure 4: **Development of the boundary layer at the endwall obtained with DNS. The contour plot shows the shape factor H_{12} with selected levels being indicated $H_{12} = 1.6$ highlighted by an isoline. Selected streamlines highlight physical differences between the two cases: (a) *Tnw* DNS, (b) *T40-20* DNS. Streamlines were obtained from time averaged velocity components in $x-$ and $y-$ direction.**

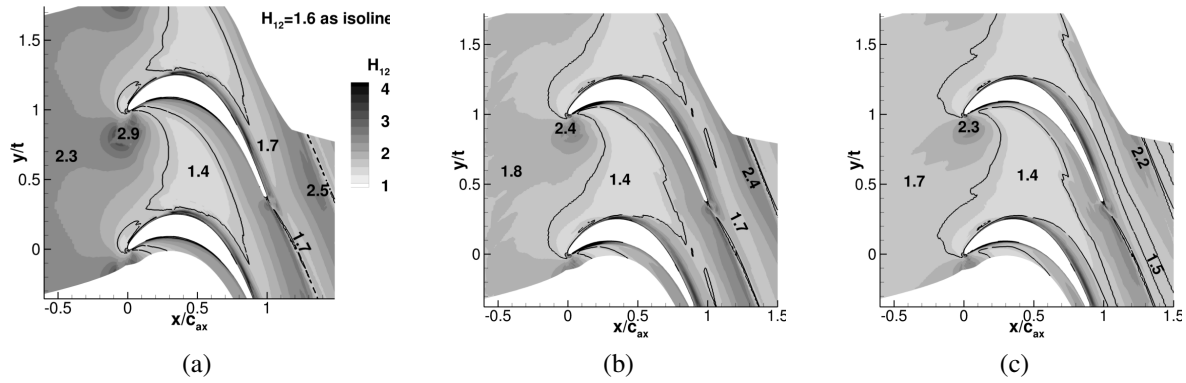

Figure 5: **Development of the boundary layer at the endwall obtained with RANS and U-RANS. The contour plot shows the shape factor H_{12} with selected levels being indicated $H_{12} = 1.6$ highlighted by an isoline: (a) *Tnw* RANS, (b) *T80-20* U-RANS, (c) *T40-20* U-RANS.**

downstream. Still further downstream, the shape factor in the crossflow boundary layer increases slowly to $H_{12} \approx 1.7$ indicating that a turbulent boundary layer prevails downstream in the passage.
More relevant differences in the endwall region are observed for the unsteady cases investigated. For the time-averaged DNS predictions in Figure 4b, the incoming wakes produce an increased boundary layer thickness and a smaller shape factor around, $H_{12} \approx 2.3$, in front of the cascade when compared to the *Tnw* case. With the wakes, the saddle point is shifted nearer to the leading edge and the shape factor decreases in the front area of the leading edge from $H_{12} \approx 4$ to $H_{12} \approx 2.5$. The turbulent strip after the lift-off line between pressure side and suction side becomes smaller. The formation of the endwall crossflow seems to be unaffected by the passing wakes.
The time-averaged values of H_{12} near the endwall obtained by the U-RANS calculations for the two unsteady configurations in Figure 5b and 5c show a larger impact of the periodical passing wakes on the inflow endwall boundary layer with $H_{12} \leq 1.8$ in both cases. The highest H_{12} values remain in the front region of the leading edge. A change of the Strouhal number has no noticeable effect on

the boundary layer as confirmed by comparing Figure 5b and Figure 5c. The higher frequency of the wakes only leads to a more frequent disturbance of the inlet boundary layer. The consequence in the time average is a reduction of the shape factor in front of the cascade and a larger extension of the turbulent strip downstream in the passage. For both U-RANS configurations, the passing wakes seem to influence the endwall boundary layer in the entire cascade in contrast to the DNS predictions where the effects of the incoming wake on the endwall boundary layer are limited to the front of the cascade and at the entry into the passage.

For a quantitative evaluation of the boundary layer development in the passage, the one-dimensional pitch-wise averaged profiles of u_t, the tangential component of the velocit, and of the turbulent kinetic energy (TKE) are shown at six different locations in Figure 6. In the DNS (Figure 6a), between

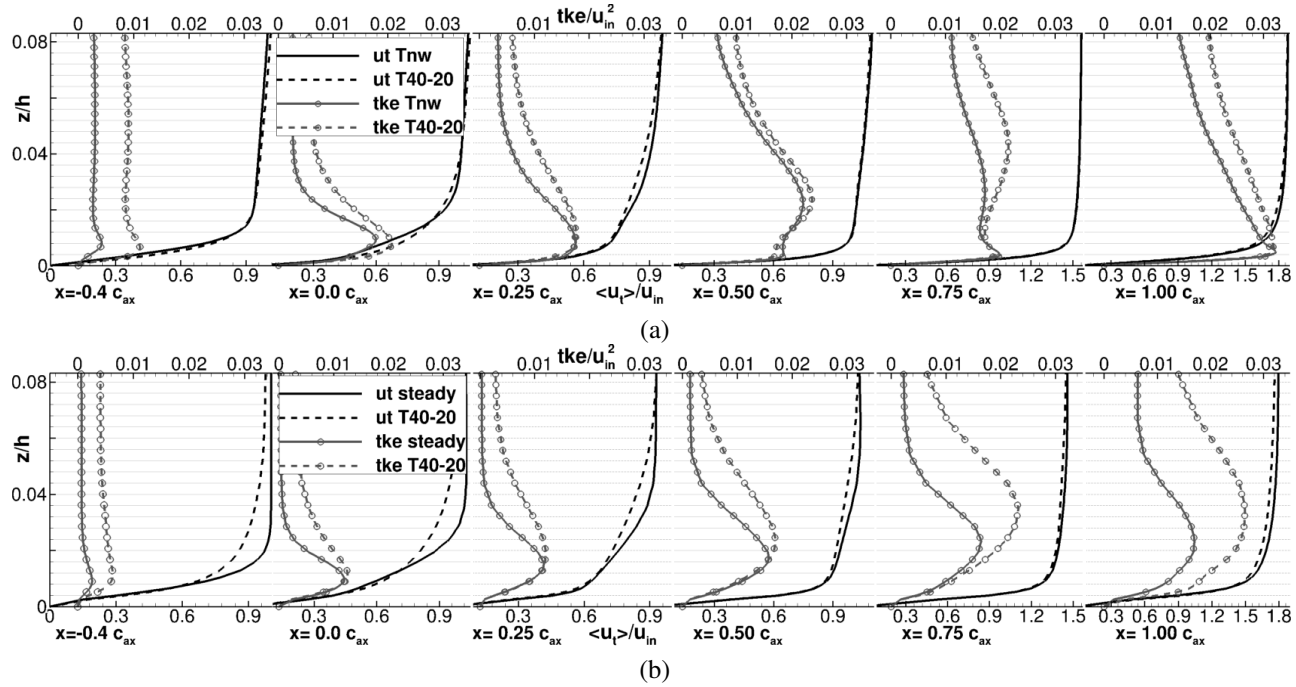

Figure 6: **Span-wise averaged tangential velocity u_t and TKE at six different locations $x/c_{ax} = -0.4,\ 0,\ 0.25,\ 0.5,\ 0.75,$ and 1.0. Comparison between case *Tnw* and case *T40-20* (a) DNS, (b) URANS.**

$x = -0.4\,c_{ax}$ and $x = 0\,c_{ax}$ the profile of the pitch-wise averaged velocity exhibits an increasing thickness. In this region, the influence of the wakes on u_t is small. However, the presence of the wakes results in higher TKE at $x = -0.4\,c_{ax}$ both for the free stream and for the boundary layer. The velocity gradient near the endwall leads to production of TKE. Between $x = -0.4\,c_{ax}$ and $x = 0\,c_{ax}$ the peak of the TKE in the boundary layer increases by a factor about 4 in the case *Tnw* DNS, from TKE ≈ 0.004 to TKE ≈ 0.017. Near the endwall, the impact of wakes on the TKE decreases. Further downstream, at $x = 0.25c_{ax}$, around the position of the turbulent strip, the endwall crossflow can be observed according to the kink of the u_t-profile at $z/h \approx 0.01$. The development of the endwall crossflow can be detected from this point to the outlet of the cascade at $x = 1\,c_{ax}$ as it leads to a much fuller velocity profile. Along this part of the passage, a first peak of the incoming TKE is lifted off the wall and broadens, while a second peak of TKE grows close to the endwall. This process is unaffected by the presence of the wakes. Furthermore, the velocity profiles coincide in both cases with and without wakes.

The evolution of the velocity profiles for the RANS and the U-RANS simulations in Figure 6b is sim-

ilar to the DNS results in Figure 6a. Slight differences occur in the upstream part due to the different inflow conditions. The impact of the wakes on the mean velocity appears to be larger here. Further downstream this difference disappears, but the near-wall velocity gradient is smaller than obtained with DNS. The TKE behaves similarly to the DNS case up to $x \approx 0.25\, c_{ax}$. Further downstream the peak of TKE moves away from the wall as in the DNS case, but increases in value. The near-wall peak observed with DNS is not created. Overall, the wakes have a stronger influence on TKE in the URANS simulation.

The effects of the incoming wakes on the time-averaged wall shear stress are presented in Figure 7

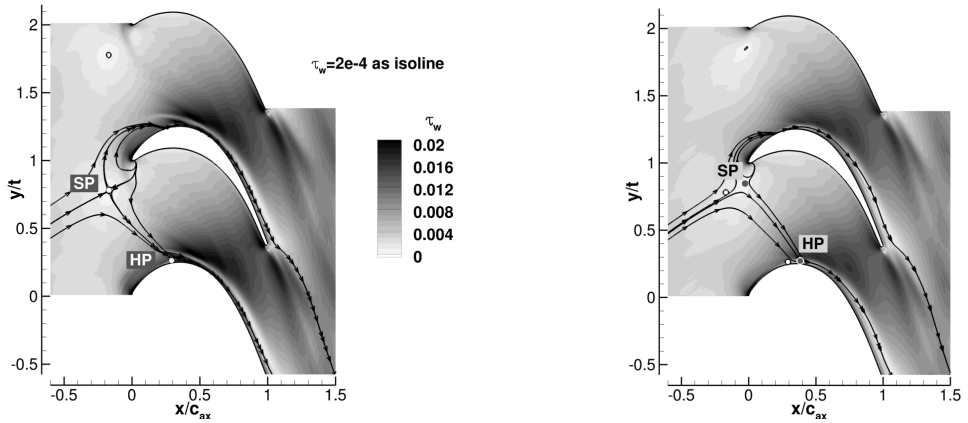

Figure 7: **Development of the shear stress at the endwall through the cascade and selected streamlines as computed with DNS: (a) DNS case *Tnw*, (b) DNS case *T40-20*.**

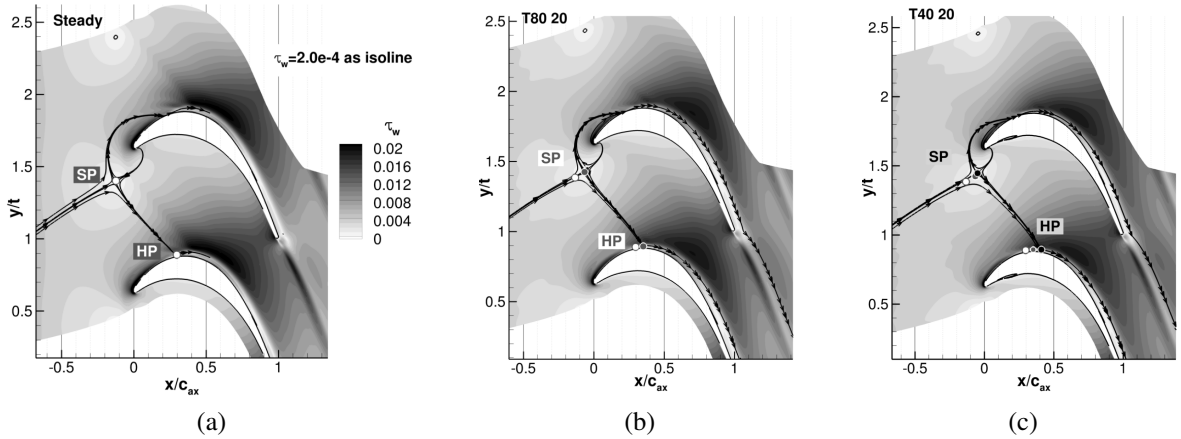

Figure 8: **Development of the shear stress at the endwall through the cascade and selected streamlines as computed with (U)RANS: (a) RANS case *Tnw*, (b) U-RANS case *T80-20*, (c) U-RANS case *T40-20*.**

and 8. As already described above, due to the two opposing effects the presence of the wakes increases only slightly the wall shear stress in front of the passage. In the narrowest cross-section of the passage near the suction side and near the trailing edge on the pressure side, the wall-shear stress decreases. Here, the flow undergoes strong acceleration. Hence, the turbulence intensity of the incoming wakes decreases. However, the reducing effect of the velocity deficit of the wakes on the wall

shear stress remains. The result is a reduction of the wall shear stress on the endwall.
The comparison of the time-averaged velocity streamlines near the endwall between the DNS and the RANS/U-RANS illustrates further effects produced by the incoming wakes. The influence of the wakes on the position of the saddle points (SP) and the lift-off line is similar for the DNS and the U-RANS predictions. For both, the saddle points are moving closer to the cascade leading edge by the wakes. The lift-off line is shifted in axial direction in the cascade passage and the impact with the adjacent suction side (HP) occurs more downstream. The displacement of the points HP and SP, which is caused by the presence of the wakes, is the same for the U-RANS simulation and the DNS. The Strouhal number of the U-RANS simulation *T80-20* is between the other two investigated cases *Tnw* and *T40-20*. Therefore, it is not surprising that the effects of the wakes occur in some attenuated form compared to the *T40-20* simulation.

Phase-averaged data for case *T40-20*

Figure 9 shows phase-averaged data obtained from DNS via explicit phase averaging for different instants during a period. Figure 10 shows the same data obtained from one period of the U-RANS simulation. The positions of the two wakes per blade passage of the *T40-20* configuration are visible in front of the cascade. In the first picture, one of the wakes is reaching the suction side near the leading edge and the other is in the middle of the passage. In the second picture, the first wake is in front of the leading edge and the second is moving more into the passage. In the third and the fourth pictures, the first wake is directed to the leading edge on the pressure side and the other moves towards to an acceleration near the suction side.
The incoming wakes cause a stronger impact on the predicted U-RANS shape factor H_{12} compared to the DNS phase-averaged results for the same phase Φ. The turbulent strip detected in the DNS by the shape factor $H_{12} < 1.6$ between the leading edge on the pressure side and the suction side remains present throughout and is only weakly influenced by the incoming wakes. For the DNS downstream of the turbulent strip, the shape factor distributions do not show relevant periodical disturbance of the endwall boundary layer caused by the wakes. For the U-RANS, the predicted shape factor H_{12}, and consequently the endwall boundary layer, seems to be more influenced by the incoming wakes. In front of the leading edge, in the U-RANS simulations, the shape factor H_{12} shows smaller values where the wake interacts with the incoming endwall boundary layer, like for the DNS. Near the saddle point region an increase of the shape factor is observed for both simulation approaches. The difference of the U-RANS with respect to the DNS results becomes relevant only after the turbulent strip. For the U-RANS the oscillations of the extension of this turbulent strip region cause a periodic variation in the entire passage.
For the DNS and the U-RANS simulations an oscillation of the saddle point position is induced by the passing wakes as illustrated in Figures 9b and 10b. There, the white and red points near the leading edge indicate the time-averaged saddle point positions for the case *Tnw* and the case *T40-20*. The third picture, for $\Phi = 3/4\,T$, shows the nearest position of the saddle point to the leading edge for both methods. Furthermore, the incoming wakes influence the position of the lift-off lines and the relative interaction position on the suction side as discussed in the previous subsection. The wall shear stress near the suction side is periodically influenced by the passing wakes. The negative effects on the inlet and the positive effects in the passage of the wakes on the wall shear stress described in the previous subsection can also be confirmed by the figures presented, in the DNS results a little clearer than in the U-RANS results.

CONCLUSIONS

DNS and U-RANS simulations were used to investigate the flow through a linear T106 LPT cascade near the endwall affected by periodic incoming passing wakes. The influence of the wakes

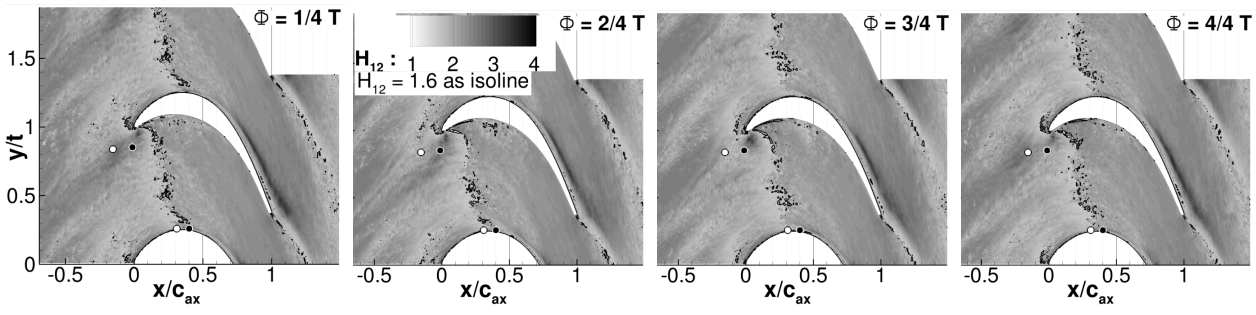

(a)

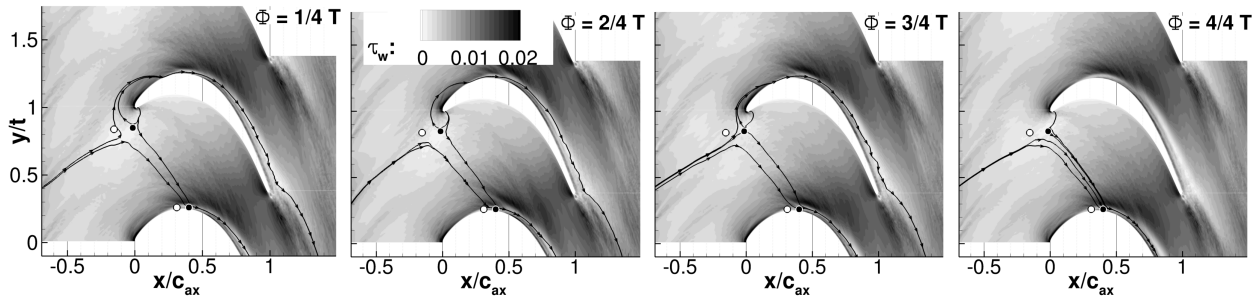

(b)

Figure 9: **Phase-averaged data at the endwall from DNS of the case *T40-20* for** $\phi = 1/4T,\ 1/2T,\ 3/4T,\ T$**: (a) shape factor, (b) the dimensionless wall shear stress and the lift-off lines at the endwall through the cascade.**

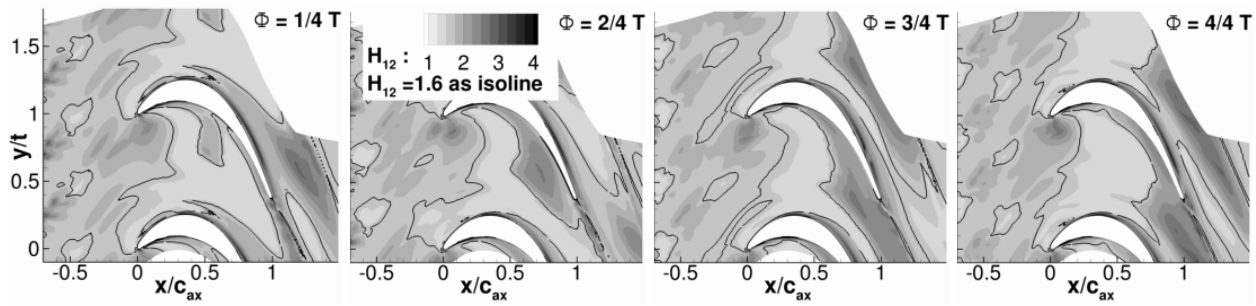

(a)

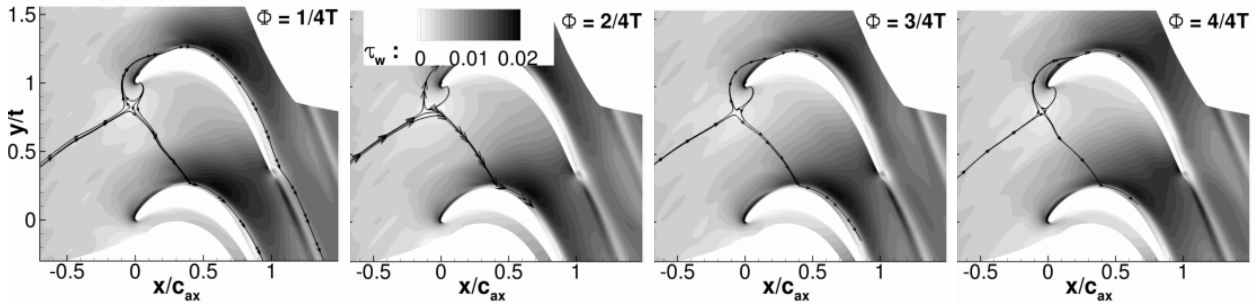

(b)

Figure 10: **Phase-averaged data at the endwall from U-RANS simulation of the case *T40-20* for** $\phi = 1/4T,\ 1/2T,\ 3/4T,\ T$**: (a) shape factor, (b) the dimensionless wall shear stress and the lift-off lines at the endwall through the cascade.**

on the secondary flow was evaluated comparing the flow without and with periodical wakes. The analysis of the time-averaged and phase-averaged boundary layer parameters for the investigated configurations allows to draw the following conclusions by means of the DNS results:

- In the inflow, the impact of the wakes on the incoming boundary layer only results in additional turbulence at the position of the wakes. The shape factor and the wall shear stress are only weakly influenced by the wakes.
- In front of the cascade, the periodical wakes make the saddle point move to the leading edge.
- The lift-off line close to the leading edge of the blades and in the passage is shifted in axial direction.
- Within the cascade, a turbulent strip across the passage is detected by using the shape factor H_{12}. Its position at $x \approx 0.25\, c_{ax}$ is only weakly affected by the wakes.
- Downstream of the turbulent strip, the boundary layer of the endwall crossflow is not influenced by the periodical upstream wakes.

Moreover concerning the comparison between the DNS and U-RANS predictions:

- The RANS/U-RANS predicts well the mean velocity development in the passage, but differs in the evolution of the turbulent kinetic energy through the passage. In the case with and without wakes, the commonly used $k-\omega$ turbulence model and the $\gamma - Re_{\theta t}$ transition model have difficulties to accurately predict the extension of the turbulent strip detected by the DNS and consequently to match the development of the boundary layer of the endwall crossflow.

These observations are valid for the studied configuration, where the incoming boundary layer thickness is smaller than 6% of the half span of the profile. For more realistic cases with $\delta/h \approx 0.25$ a stronger influence of the wakes on the inflow boundary layer is expected. Further work is under way to understand if and how the endwall flow in the passage is affected by this modification.

ACKNOWLEDGEMENTS

The present work is funded by the German Research Foundation (DFG) via the project PAK530. The DNS were performed on a Bull HPC-Cluster and on an SGI Altix system at the Center for Information Services and High Performance Computing (ZIH) at TU Dresden. Dr. Wissink kindly provided the time signal data of the cylinder wake. The authors wish to acknowledge DLR Cologne, Institute of Propulsion Technology, for provision of the numerical flow solver TRACE.

References

Ciorciari, R., Kirik, I., and Niehuis, R. (2014). Effects of unsteady wakes on the secondary flows in the linear T106 turbine cascade. *ASME Journal of Turbomachinery*, 136(9).

de Meux, B. D. L., Audebert, B., and Manceau, R. (2012). Anisotropic linear forcing for synthetic turbulence generation in hybrid RANS/LES modelling. *9th International ERCOFTAC Symposium on Engineering Turbulence Modelling and Measurements*. Thessaloniki, Greece.

Denton, J. and Pullan, G. (2012). A numerical investigation into the source of endwall loss in axial flow turbine. *ASME Paper GT2012-69173*.

Harrison, S. (1989). Secondary loss generation in a linear cascade of high-turning turbine blades. *ASME Paper 89-GT-47*.

Hinterberger, C., Fröhlich, J., and Rodi, W. (2008). 2D and 3D turbulent fluctuations in open channel flow with Re_τ=590 studied by Large Eddy Simulation. *Flow, Turbulence and Combustion*, 80(2):225–253.

Holley, B. M., Becz, S., and Langston, L. S. (2006). Measurement and calculation of turbine cascade endwall pressure and shear stress. *ASME Journal of Turbomachinery*, 128(2):232–239.

Koschichow, D., Kirik, I., Fröhlich, J., and Niehuis, R. (2014). DNS of the flow near the endwall in a linear low pressure turbine cascade with periodically passing wakes. *ASME Paper GT2014-25071*.

Kožulović, D. (2007). *Modellierung des Grenzschichtumschlags bei Turbomaschinenströmungen unter Berücksichtigung mehrerer Umschlagsarten*. Phd thesis, Ruhr-Universität Bochum.

Langston, L. (1980). Crossflows in a Turbine Cascade Passage. *Journal of Engineering for Power*, 102:867–874.

Lei, Q., Zhengping, Z., Huoxing, L., and Wei, L. (2010). Upstream wake-secondary flow interactions in the endwall region of high-loaded turbines. *Computers and Fluids*, 39(9):1575–1584.

Marciniak, V., Kugeler, E., and Franke, M. (2010). Anisotropic linear forcing for synthetic turbulence generation in hybrid RANS/LES modelling. *V European Conference on Computational Fluid Dynamics ECCOMAS CFD*. Lisbon, Portugal.

Michelassi, V., Chen, L.-W., Pichler, R., and Sandberg, R. D. (2014). Compressible direct numerical simulation of low-pressure turbines: Part II - effect of inflow disturbances. *ASME Paper GT2014-25689*.

Michelassi, V., Martelli, F., Dénos, R., Arts, T., and Sieverding, C. H. (1999). Unsteady heat transfer in stator-rotor interaction by two-equation turbulence model. *ASME Journal of Turbomachinery*, 121(3):436–447.

Perdichizzi, A. (1986). Mach number effects on secondary flow development downstream of a turbine cascade. *ASME Paper 89-GT-67*.

Schobeiri, M. T. and Nikparto, A. (2014). A comparative numerical study of aerodynamics and heat transfer on transitional flow around a highly loaded turbine blade with flow separation using rans, urans and les. *ASME Paper GT2014-25828*.

Travin, A., Shur, M., Spalart, P., and Strelets, M. (2004). On urans solutions with les-like behaviour. *Congress on Computational Methods in Applied Sciences and Engineering, ECCOMAS2004*.

Tucker, P. (2011). Computation of unsteady turbomachinery flows: Part 1– Progress and challenges. *Progress in Aerospace Sciences*, 47:522–545.

Tyacke, J., Tucker, P., Jefferson-Loveday, R., Vadlamani, N. R., Watso, R., Naqavi, I., and Yang, X. (2013). LES for turbines: methodologies, cost and future outlooks. *ASME Paper GT2013-94416*.

Wissink, J. and Rodi, W. (2008). Numerical study of the near wake of a circular cylinder. *International Journal of Heat and Fluid Flow*, 128(4):668–678.

Yang, H., Kuegeler, E., and Weber, A. (2002). Conservative zonal approach with appllications to unsteady turbomachinery flows. *DGLR Jahrestagung*, DGLR-JT2002-073. Stuttgart, Germany.

Yang, H., Nuernberger, D., and Kersken, H.-P. (2006). Toward excellence in turbomachinery Computational Fluid Dynamics: A hybrid structured-unstructured Reynolds-Averaged Navier-Stokes solver. *Journal of Turbomachinery*, 128(2):390–402.